Available online at www.sciencedirect.com
ScienceDirect
Analytical Biochemistry 367 (2007) 28–39
ANALYTICAL BIOCHEMISTRY
www.elsevier.com/locate/yabio

Inaccuracies in selected ion monitoring determination of isotope ratios obviated by profile acquisition: nucleotide $^{18}O/^{16}O$ measurements ☆

Adam G. Cassano [a,1], Benlian Wang [b], David R. Anderson [a], Stephen Previs [c], Michael E. Harris [a], Vernon E. Anderson [a,*]

[a] Center for RNA Molecular Biology, Case Western Reserve University School of Medicine, Cleveland, OH 44106, USA
[b] Department of Biochemistry, Case Western Reserve University School of Medicine, Cleveland, OH 44106, USA
[c] Department of Nutrition, Case Western Reserve University School of Medicine, Cleveland, OH 44106, USA

Received 5 December 2006
Available online 2 April 2007

Abstract

Precise and accurate measurements of isotopologue distributions (IDs) in biological molecules are needed for determination of isotope effects, quantitation by isotope dilution, and quantification of isotope tracers employed in both metabolic and biophysical studies.While single ion monitoring (SIM) yields significantly greater sensitivity and signal/noise than profile-mode acquisitions, we show that small changes in the SIM window width and/or center can alter experimentally determined isotope ratios by up to 5%, resulting in significant inaccuracies. This inaccuracy is attributed to mass granularity, the differential distribution of digital data points across the m/z ranges sampled by SIM. Acquiring data in the profile mode and fitting the data to an equation describing a series of equally spaced and identically shaped peaks eliminates the inaccuracies associated with mass granularity with minimal loss of precision. Additionally a method of using the complete ID profile data that inherently corrects for "spillover" and for the natural-abundance ID has been used to determine $^{18}O/^{16}O$ ratios for 5′,3′-guanosine bis-[$^{18}O_1$]phosphate and TM[$^{18}O_1$]P with precisions of ~0.005. The analysis protocol is also applied to quadrupole time-of-flight tandem mass spectrometry using [2-^{18}O]arabinouridine and 3′-UM[$^{18}O_1$]P which enhances signal/noise and minimizes concerns for background contamination.

Keywords: Isotope ratio; Isotopologue distribution; Mass isotopomer distribution; Tandem mass spectrometry; Heavy atom isotope effect; Oxygen-18; Nucleotide; Mass granularity; Whole-molecule mass spectrometry

Heavy atom isotope effects generated by substituting ^{13}C, ^{15}N, or ^{18}O are important tools for probing the mechanisms and transition states of chemical reactions [1], including enzyme-catalyzed reactions [2–7]. Because the observed effects for isotopic substitution of heavy atoms are extremely small, typically a few percent, they cannot be determined by direct comparison of experimentally determined rate constants. Instead, heavy atom isotope effects are generally measured by internal competition methods that compare the isotopic composition of the reactant and the product [3,8]. These measurements require the ability to determine isotope ratios with precisions better than 1%. Such performance is typically achieved using isotope ratio mass spectrometry (IRMS)[2] or dual-label

☆ This work was supported by NIH Grants GM56740 (M.E.H.) and R33 DK07029 (V.E.A. and S.P.) and a HHMI predoctoral fellowship (A.G.C.).
* Corresponding author. Fax: +1 216 368 3419.
E-mail address: vernon.anderson@case.edu (V.E. Anderson).
[1] Current address: Department of Chemistry, Drew University, Madison, NJ 07940, USA.

[2] *Abbreviations used:* IRMS, isotope ratio mass spectrometry; ESI, electrospray ionization; ID, isotopologue distribution; IIC, isotopologue ion cluster; MALDI, matrix-assisted laser desorption ionization; QMS, quadrupole mass spectrometry; SIM, selected ion monitoring; TOF, time-of-flight.

0003-2697/$ - see front matter © 2007 Elsevier Inc. All rights reserved.
doi:10.1016/j.ab.2007.03.037

scintillation counting of radioactive isotopes [3,9]. While these methods have proven useful, both possess inherent limitations that restrict their application. IRMS can analyze only small, nonpolar gasses such as CO_2, N_2, and H_2; thus, this technique can be used only when the atom of interest can be quantitatively converted to one of these gasses. Scintillation counting requires substantial double-labeling schemes involving specific isotopic pairs (usually ^3H and ^{14}C, although others can be used [10]), again limiting the molecules that can be analyzed.

One alternative to these methods is whole molecule mass spectrometry, a technique that was used as early as the 1970s for isotope ratio analysis of formyl-methyl ester and ethanol by gas chromatography quadrupole mass spectrometry (QMS) [11,12]. Today, the development of gentler ionization methods such as electrospray ionization (ESI) and matrix-assisted laser desorption ionization (MALDI) allow larger molecules to be analyzed. Coupled with QMS, ESI makes possible the analysis of isotope ratios for numerous biologically relevant organic molecules with molecular masses in excess of 500 Da [13–16]. However, several design features prevent QMS from achieving the precision and accuracy obtained by IRMS. The sources of error in the ESI–QMS isotope ratio measurements include noise (from both the ion source and the detector), background, intensity fluctuations, and the inability to capture the entire ion current arising from individual isotopologues.[3] Some of these effects can be minimized by working with isotope ratios near unity, utilizing background subtraction and/or injecting analyte by continuous direct infusion.

To enhance sensitivity, with concomitant improvements in signal/noise and precision, isotope ratio QMS studies often use single ion monitoring (SIM) to maximize the amount of time that the QMS acquires data with the greatest intensity from the isotopologue peaks of interest. With singly charged ions, the peaks of an isotopologue ion cluster (IIC) are separated by integral increments in m/z. While SIM acquisitions maximize the sensitivity of detection, the studies presented herein demonstrate that this approach is inherently problematic since current QMS instruments collect data at digitally determined, discrete m/z values which introduces a mass granularity. A result of this mass granularity is that the separation between the discrete m/z values that are analyzed does not permit the peaks arising from individual isotopologues to be sampled at identical positions across the peak. This inherent feature of QMS can compromise the accuracy of isotope ratios measured by SIM [17]. In our studies, shifting the center of the m/z range monitored in SIM analyses by as little as 0.01 could result in variations in the measured isotope ratio of up to 5%. These variations appear to result from differences in the number of the digitized m/z data points averaged by the SIM function for different peaks in the IIC as implemented by the Finnigan Xcalibur software. We demonstrate that this technical difficulty is alleviated by acquiring data in the Profile-Scan mode and fitting the resulting profile data to an equation that accurately describes a series of identically shaped peaks that comprise the IIC. The equation resulting from the fitting process is analytically integrated to determine the relative areas of each peak in the ID, which provides the necessary data to calculate the isotope effect. While the precision obtained by this method is slightly less than that which might be obtained by IRMS, the protocol described here removes a critical source of inaccuracy and yields isotope ratios of sufficient precision for analysis of isotope effects as small as 1.005. Importantly, the ability to analyze isotope ratios in nucleotides will permit the application of heavy atom isotope effect studies to enzymes involved in DNA and RNA metabolism.

Time-of-flight mass analyzers, now routinely available both as MALDI-TOF and as the mass analyzer for tandem mass spectra in Q-TOF instruments, inherently generate profile scan data so the procedure described is readily applicable to time-of flight data. The peak fitting algorithm developed obviates the necessity of correcting for overlapping peaks in the IIC. An additional benefit of the algorithm presented is that it fits the entire IIC of the labeled compound with its enrichment as the sole variable, automatically accounting for the natural-abundance contribution to the ID based on the elemental composition of the analyte.

Materials and methods

5′-Thymidine mono[nonbridging-$^{18}O_1$]phosphate

Samples of ^{18}O-enriched thymidine monophosphate (TMP) were prepared by hydrolysis of thymidine-5′-*p*-nitrophenyl phosphate (Sigma) in $H_2{}^{18}O$ (~50%) water (Isotec) catalyzed by 0.3 M $MgCl_2$, pH 9.1 (50 mM Tris–HCl) [18]. Hydrolysis reactions were placed in flame-sealed glass ampoules and incubated at 37 °C in a dry incubator for 62 days.

5′,3′-Guanosine bis[5′nonbridging-$^{18}O_1$]phosphate

Samples of ^{18}O-enriched pGp were prepared enzymatically by incubating pre-tRNA^{asp} from *Bacillus subtilis* (pre-tRNA) with *Escherichia coli* ribonuclease P (RNase P) in $H_2{}^{18}O$ (~50%) water. RNase P reactions, 50 mM 4-morpholineethane sulfonic acid, pH 6, 1 M NaCl, and 25 mM $MgCl_2$ were thermostatted at 37 °C [19]. RNAs were synthesized by in vitro transcription essentially as described [20]. RNAs were purified by denaturing polyacrylamide gel electrophoresis using gels containing 6% acrylamide and 7 M urea (National Diagnostics). RNA

[3] Isotopologues are molecules that differ by the presence of different isotopes resulting in an isotopologue ion cluster in mass spectra. The areas of all of the isotopologue peaks comprise the isotopologue distribution (ID). The area of the peak associated with each isotopologue is denoted M_n, where n is the number of neutrons in excess of that present in the monoisotopic mass ion, M_0.

was visualized by UV shadowing, excised from the gel, and eluted into 0.3 M sodium acetate, 10 mM Tris–HCl (pH 8), 1 mM EDTA, and 0.1% SDS overnight. After hydrolysis catalyzed by RNase P, the tRNA product with a single ^{18}O incorporated into the scissile phosphate was purified by gel electrophoresis prior to digestion overnight with 17 units of ribonuclease T_2 in 50 mM NaOAc, pH 4.7, generating the unique [5′-$^{18}O_1$]pGp.

[2-^{18}O]Arabinouridine

[2-^{18}O]Arabinouridine was generated by hydrolysis of 250 μmol of 2,2′-anhydrouridine (Sigma) with 10 mM sodium hydroxide in dimethylformamide for 5 h at 65 °C. Arabinouridine was purified from unreacted anhydrouridine by HPLC.

3′-Uridine-[nonbridging-$^{18}O_1$]phosphate

To enrich one of the nonbridging oxygens of 3′-UMP with ^{18}O, 2′,3′-cyclic UMP was hydrolyzed in base (pH 9.5) in $H_2{}^{18}O$. The reaction was incubated overnight at 65 °C and the resultant 2′-UM[nonbridging-^{18}O]P and 3′-UM[nonbridging -^{18}O]P were resolved by HPLC.

HPLC purification of nucleosides and nucleotides

3′-UM[$^{18}O_1$]P, 5′-TM[$^{18}O_1$]P, and [5′-$^{18}O_1$]pGp were purified by HPLC (300 mm × 3.9 mm, 10 μm C_{18} packing) eluted isocratically using 50 mM diisopropylethylamine (Aldrich), 1% acetic acid in water (pH 4.3) as the mobile phase. For [2-^{18}O]uridine, samples were resolved by a gradient of acetonitrile in 0.2 M ammonium acetate (5–20% acetonitrile in 60 min). Appropriate fractions containing either uridine, UMP, TMP, or pGp were collected. Samples were desalted using multiple rounds of lyophilization and resuspension in water. Prior to mass spectrometric analysis, TMP samples were resuspended in methanol:water (50:50) to a concentration of ∼50 μM and pGp samples were resuspended in methanol:water:acetic acid (50:50:0.1) to a concentration of ∼100 μM.

Electrospray ionization quadrupole mass spectrometry

ESI–QMS measurements were performed using a Finnigan TSQ 7000 instrument controlled by Xcalibur software in negative ion mode. Samples were injected by direct infusion, with flow rate at 10 μL/min. The electron photomultiplier voltage was 1440 V and the pcthresh signal cutoff was set to 4000. Care was taken to ensure that at the selected pcthresh cutoff, signal noise could be observed even with the source voltage turned off to ensure linearity, even at low signal intensities. The default value of pcthresh was too large and preferentially reduced the intensity of low-abundance peaks in the IIC. The capillary temperature for the ion source was 250 °C. Unless specified, SIM acquisitions were performed by entering a 0.1-m/z window, which the Xcalibur software defaulted to the minimum 0.16 m/z, and a 0.1-s dwell time. Centers for SIM acquisitions were varied as indicated and Results and discussion. Narrow-range-profile SIM scans were acquired to characterize the number of m/z settings used as a function of SIM width and center. Scan acquisitions for pGp covered a range of 439–449 m/z in one second with nominally 25 data points for each increment of 1 m/z. Scan acquisitions for TMP covered 318–328 m/z in 1 s with nominally 250 points. Data for all acquisitions were averaged over >200 scans. For both types of acquisitions, blank acquisitions, consisting of either methanol:water:acetic acid (50:50:0.1) for pGp samples or methanol:water (50:50) for TMP samples, were subtracted from the sample acquisitions.

Time-of-flight mass spectrometry

The application of the analysis of isotope ratios by analysis of IDs was extended to tandem-quadrupole time-of-flight mass spectrometry by analysis of [2-^{18}O]arabinouridine and UM[$^{18}O_1$]P with an Applied Biosystems Q-STAR. All analyses were performed by direct infusion of the nucleoside/nucleotide in 50% acetonitrile 1% formic acid. To determine that the complete IIC is passed through the quadrupole with no fractionation the collision energy was set at 5 V, the mass window center was set in the middle of the IIC, and the low-resolution setting was increased until the relative intensities of the cluster peaks became invariant. The collision energy was then varied to optimize the intensity of the product ion to be analyzed. A series of tandem mass spectra of [2-^{18}O]arabinouridine and UM[$^{18}O_1$]P, ∼50 μM, were acquired with the $^{18}O/^{16}O$ ratio varied by serial additions of ^{18}O-labeled material. The time-of-flight spectra were fit to a series of Gaussian peaks as described below.

Nonlinear curve fitting

The relative areas of peaks in an identified IIC were determined by nonlinear least squares analysis using Origin software. For profile data acquired with different mass spectrometers, the first task is to determine the peak shape. Our data from time-of-flight mass spectrometers, including both MALDI and ESI sources, yielded best fits to Gaussian peak shapes. The individual isotopic peaks in the profile data obtained by ESI–QMS were asymmetric leading peaks typical of quadrupole mass filters [21] but were well fit by an asymmetric double sigmoidal equation where the different leading and lagging exponential decays were accounted for by the terms w2 and w3, respectively, as shown in Eq. (1).

$$y = B + A\left(\frac{1}{1+e^{-(x-x_c+w1/2)/w2}}\right)\left(1-\frac{1}{1+e^{-(x-x_c-w1/2)/w3}}\right). \quad (1)$$

All of the profile data points were included in the analysis. Eq. (2) then describes the entire IIC of n peaks where A_i

and x_{ci} represent the amplitude and center of the i^{th} peak, respectively,

$$y = B + \sum_{i=1}^{n} A_i \left(\frac{1}{1+e^{-(x-x_{ci}+w1/2)/w2}} \right) \left(1 - \frac{1}{1+e^{-(x-x_{ci}-w1/2)/w3}} \right). \quad (2)$$

Constraining w1, w2, and w3 to be invariant results in identically shaped peaks, while for Gaussian peaks only the peak width needs to be invariant. The centers of the individual peaks, x_{ci}, may be fixed at a constant interval (typically 1.000 m/z for singly charged ions). These assumptions are based on the premise that the features of the mass separation that lead to peak broadening will behave identically for the molecules containing heavy isotopes.[4] This simplification of the fitting procedure is validated by the excellent fits obtained. The areas corresponding to the individual sequential peaks of the IIC are proportional to the amplitudes, A_i. Two advantages of this procedure are that (1) peak overlaps are correctly accounted for and (2) no peak truncation is required.

Simulated mass spectra

To investigate the required signal/noise and the effects of mass granularity, simulated IDs were generated using Excel. IDs were generated according to Eq. (3); noise was added using the random number function "RAND(#)" whose values were scaled to obtain the desired S/N.

$$f(x) = \sum_{i=1}^{n} \{ (A_i \times \text{peakshape function}) + \text{RAND}(\#) \}. \quad (3)$$

When random error was introduced, each simulation was run five times. When analyzing mass granularity, the data points were separated by 0.039 m/z and distributed so that a data point was positioned at the maximal y value for the second isotopic peak.

Prediction of IDs

As described in the accompanying paper [22], the area of each peak in the ID normalized to the area of the monoisotopic mass peak, M_0, can be calculated from the elemental composition of the analyte by Eq. (4),

$$M_n/M_0 = m_1^n (0.99)^{n-1} \sum_{i=0}^{n/2} (m_2/m_1^2)^i/(n-2i)!i!,$$
$$m_1 = \sum_{\text{elements}} ex_{e1}/x_{e0}, \quad m_2 = \sum_{\text{elements}} ex_{e2}/x_{e0} \quad (4)$$

where M_n/M_0 is the area of the peak in the ID that has n neutrons in excess of the monoisotopic mass, normalized to the M_0, and m_1 *and* m_2 are determined by the number of atoms of each element present, e, and the natural abundance of the elements containing 0, 1, and 2 additional neutrons, represented by the mol fractions x_{e0}, x_{e1}, and x_{e2}, respectively. When a sample enriched at a limited number of sites is being analyzed, which is the case in isotope effect studies, and when isotope-coded affinity tags are employed in proteomics [23], the observed ID is a summation of the natural-abundance IDs for the unlabeled compound and each enriched peak whose contributions are weighted by their ratio to the unlabeled mol fraction. In the experimental cases that we describe, each labeled compound contains a single enriched ^{18}O atom, so the prediction of the ID will be a sum of the unlabeled and labeled IDs, with the labeled ID weighted by the mol fraction ratio, X_{18}/X_{16}, as shown in Eq. (5).

$$\begin{aligned}(M_n/M_0)_{\text{pred}} &= \{(M_n/M_0)_{\text{unlableled}}\} \\ &\quad + X_{18}/X_{16}\{(M_{n'}/M_0)_{^{18}O_1}\} \\ &= m_1^n (0.99)^{n-1} \sum_{i=0}^{n/2} (m_2/m_1^2)^i/(n-2i)!i! \\ &\quad + X_{18}/X_{16}\left\{ m_{1'}^{n'} (0.99)^{n'-1} \sum_{i=0}^{n'/2} (m_{2'}/m_{1'}^2)^i/(n'-2i)!i! \right\}. \end{aligned} \quad (5)$$

To account for the mass offset introduced by the ^{18}O-label, $n' = n - 2$ (if $n' < 0$ then $M_{n'} = 0$) while $m_{1'}$ and $m_{2'}$ are calculated with one less O atom. The experimentally sought value, X_{18} / X_{16}, is determined by minimizing the rms for the predicted and experimental IDs as shown in Eq. (6).

$$\text{rms} = \sqrt{\frac{\sum_{n=1}^{n} [(M_n/M_0)_{\text{pred}} - (M_n/M_0)_{\text{experimental}}]^2}{n-1}}. \quad (6)$$

An Excel spreadsheet that performs the calculation of m_1 and m_2 and provides a nonlinear least squares fit of an experimental ID to Eq. (6) to determine X_{18} / X_{16} is available online as Supplementary material ("^{18}O KIE calc from ID.xls").

Results and discussion

ESI–QMS analysis of isotope ratios in nucleotides

A key limitation to mechanistic studies of heavy atom isotope effects has been the requirement for the high precision afforded by IRMS which necessitates the conversion of the atom of interest in the substrates and/or products to CO_2, N_2, or H_2. Advances in ESI–MS instrumentation permit increasing precision in whole molecule measurements of isotopic composition. In addition to numerous biochemical applications, use of ESI–MS to monitor isotope ratios now allows these instruments to be used for the analysis of isotope effects of reactions involving macromolecular substrates [16,18,24,25]. These studies can be extended to numerous reactions in the metabolism of DNA and RNA which involve the hydrolysis of

[4] It is recognized at higher mass resolutions that additional peak broadening occurs in the ID due to the presence of multiple isotopologues and the differences in mass associated with the substitution of ^2H (1.006), ^{13}C (1.003), ^{15}N (0.997), and ^{18}O (2.004). In this case w will increase with n [48].

phosphodiester bonds if the IDs of nucleotides can be determined with the requisite precision.

In these reactions hydrolysis results in incorporation of a solvent water molecule into the reactive phosphate. Thus, isotope effects on this reaction can in principle be measured by comparison of the isotopic composition of the water and the product. However, the nucleophilic oxygen is one of four in the product phosphate, and additional oxygens are present on the ribose and nucleobase of the associated nucleoside. Thus, isolation of the nucleophilic oxygen for IRMS analysis would be quite challenging indeed. However, whole molecule mass spectrometry of the resultant nucleotide monophosphates (TMP and pGp) could be used to determine these effects if the $^{18}O/^{16}O$ ratio can be measured with sufficient precision and accuracy. Pursuing these studies led us to identify a significant problem associated with the accuracy of SIM measurements of isotope ratios.

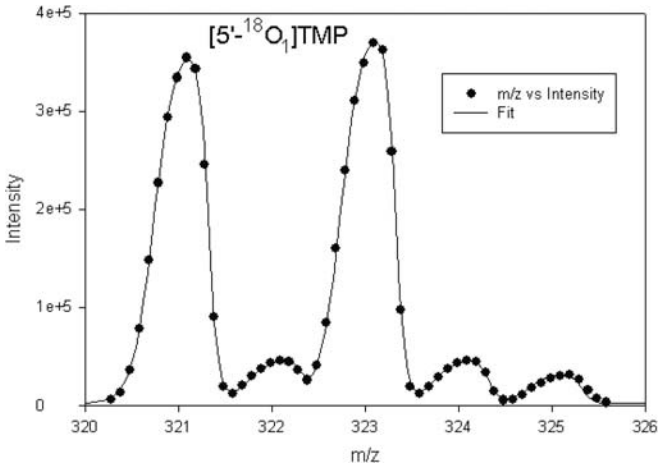

Fig. 1. Nonlinear curve fit of data from a scan acquisition of ^{18}O-enriched TMP. Data points represent the average intensity at each point for 262 scans. Data were fit to Eq. (1) describing five peaks with the baseline set to a value equal to the lowest observed intensity for the averaged scans. The R^2 for the fit was 0.9990.

Effect of mass granularity on observed isotope ratios

SIM acquisitions are routinely used to determine IDs by QMS. However, in the course of analyzing the ^{18}O content of ^{18}O-enriched 5′,3′-guanosine bis-phosphate by SIM, large effects (up to 5%) on the measured relative intensities of peaks corresponding to the M_0 (442 m/z) and M_2 (444 m/z) were observed in preliminary control analyses which resulted from uniform small changes (± 0.01 m/z) for the centers of SIM values entered in the SIM table. As shown in Table 1, when the SIM center was offset by only 0.02 there was a >2% change in the measured M_2/M_0 ratio.

The dependence of the isotope ratio on the chosen SIM values was surprising because the observed peak shapes in the M_0 and M_2 peaks are essentially identical as shown in Fig. 1. Therefore, small changes in the peak center of the same magnitude and direction were not anticipated to result in significant disparities in the measured isotope ratio. Additionally, the precision of the isotope ratio measurements for two separate pGp samples were very good when maintaining the same SIM table throughout the analysis, with standard deviations of 0.5% (Table 1S, supplementary material). These two observations strongly suggest that the differences in the measured M_2/M_0 ratios result not from a lack of precision in the measurements but from an error in accuracy. This is a particularly pernicious problem, as on any given day a test of linearity with isotope dilution may work very well, and in subsequent days a shift in calibration of 0.02 m/z could alter the observed ratios by as much as 5%, but the isotope dilution curves determined separately each day would both be linear.

Table 1
Changes in the relative intensities of M + 2 and M + 3 for ^{18}O-enriched pGp with 0.01 m/z shifts in SIM centers

SIM Center	X		
	442	444	445
	M_0	M_2/M_0	M_3/M_0
	Relative intensities		
X.00	100	97.59	13.7
X.01	100	97.52	13.7
X.02	100	93.45	13.5
X.03	100	93.35	13.2
X.04	100	99.96	14.11

Most commercial quadrupole mass analyzers separate ions into discrete digital m/z values. For the Finnigan TSQ 7000, 65,535 (2^{16}-1) digital values exist for an m/z range of about 2600. Thus, the difference between sequential m/z settings is approximately 0.0397. This mass granularity can influence the measured peak intensity ratios. A simulation of the calculated intensities that would be observed for two sequential isotopic peaks with a theoretical ratio of 1.000 and each data point separated by 0.0397 m/z highlights the problems introduced by mass granularity as shown in Fig. 2. The simulation demonstrates that a significant inaccuracy would be introduced if the isotope ratio were determined only by the ratio of the maximum intensity data points (i.e., $0.998/0.982 \neq 1.000$). Note also that the distribution of data points around the lower mass peak differs from that about the higher mass peak and is asymmetrical. This difference in data point distribution makes it impossible to define a set peak width for summation that will produce an accurate isotope ratio. A SIM width of 0.16 m/z, corresponding to the minimum allowed by Xcalibur software, would contain either four or five data points. Fig. 2 illustrates that this can result in substantially inaccurate relative areas (0.912 vs 0.864). Additionally, this simulation indicates that a 0.02-m/z shift in the SIM center would alter the m/z settings included in the SIM data acquisition (circled points in Fig. 2). The change in data points included in the SIM average again alters the calculated M_2/M_0 ratio. These

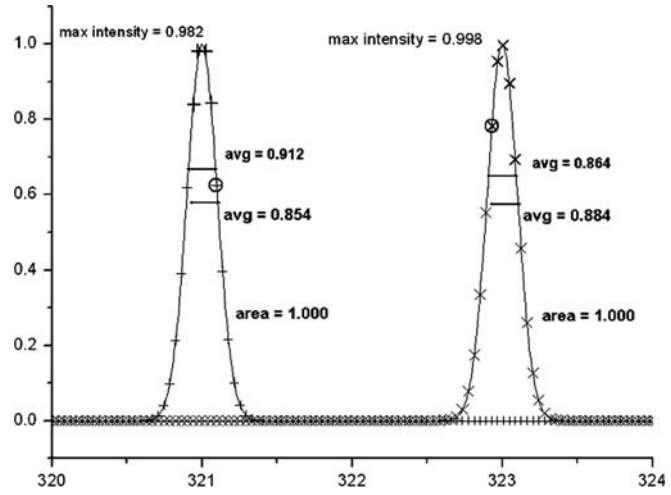

Fig. 2. Simulated distribution of the digital data points for two Gaussian peaks separated by 2 on the m/z axis. To mimic the TSQ data acquisition parameters, the simulated data points (+, ×) are separated by 0.039 m/z and represent what would be perfect data obtained from two consecutive Gaussian peaks with peak centers at 321.000 and 323.000. The peak amplitudes are both 1.000, and peak widths at half-maximal values are 0.23. The three sources of inaccuracy introduced by mass granularity are highlighted. (1) The individual data points with maximum intensity miss the peak of the Gaussian by different amounts, so that the calculated isotope ratio would be in error by 1.6%. (2) The number of data points included in a SIM experiment with a width of 0.16 m/z can be different as highlighted by the boldface data points resulting in the averaged values of 0.912 and 0.864 which correspond to an inaccuracy of the calculated isotope ratio of 6%. (3) Shifting the centers of the SIM acquisition each by 0.02 m/z results in a change in the data points that are included, a gain of the circled point in M_0 and the loss of the circled point in M_2, which alters the averages of the included data points to 0.854 and 0.884 as indicated. Integrating the areas of the two Gaussian peaks generates an accurate area ratio of 1.000.

effects of mass granularity on the accuracy of the isotope ratios are exacerbated by increased resolution, so these simulated effects may be greater than those in our experimental results. Nonetheless, differences in measured isotope ratios resulting from small shifts in the center of the SIM measurements, and the consequent potential for inaccuracies, should be anticipated.

To more closely assess the two potential errors introduced by mass granularity, SIM data were acquired in profile mode allowing access to all of the data points acquired in contrast to centroid collection providing only an average of the data points. Data were acquired for TM[^{18}O]P, $m/z = 321$ and 323). Like the results for pGp, these samples displayed significant changes in the measured M_2/M_0 ratio with small changes in the SIM center (data not shown). The m/z ranges reported in the SIM profile mode provided clear evidence of the m/z settings averaged to obtain the reported intensity for each peak (Table 2). A plot of intensity against m/z obtained from the SIM-profile mode acquisition with a nominal 0.1 SIM width displays several distinct regions of relatively stable intensity with abrupt changes as indicated by arrows in Fig. 3. We attribute the abrupt changes in intensity to changes in the m/z data points associated with the SIM center, as suggested in Fig. 2. Examination of the tabular profile data indicated that the actual SIM widths always defaulted to a minimum of 0.16 m/z. This result was important because it demonstrated that each SIM acquisition (even in profile mode) required data acquisition at four or five separate m/z settings whose values were averaged and which points were included in the average could vary when the selected SIM center was translated by as little as 0.01 m/z.

Examination of the m/z ranges for each SIM peak revealed an additional concern for the determination of isotope ratios by SIM as the ranges differed for SIM peaks with centers separated by 2.000 m/z by 0.02 (Table 2). The m/z range shifts after every 0.04 increment of the SIM center. This increment coupled with the 0.02 offset results in significant changes in the M_2/M_0 ratio occurring with every 0.02-m/z change in the SIM centers, as one of the SIM ranges is changed. For example, from Table 2, analyzing the ratio of intensities at $m/z = 323$ and $m/z = 321$, measured results with the SIM center at X.00 and X.01 (where X is either 321 or 323) should produce very similar results because the same m/z ranges are analyzed for both peaks. However, once the SIM center is changed to X.02, the m/z range analyzed for the 323 peak has been shifted 0.04 m/z, whereas the m/z range for the 321 peak remains unchanged. This change in included data points will cause a significant change in the measured 323 peak intensity while the measured 321 peak intensity necessarily remains constant, thus resulting in a significant change in the measured 323/321 (i.e., M_2/M_0) ratio. Continuing to increment the SIM center, the m/z ranges for both peaks remain constant when the SIM centers are increased from X.02 to X.03 but, when increased to X.04, the m/z range now shifts only for the 321 peak, causing a second significant change in the observed M_2/M_0 ratio.

Table 2
Output m/z ranges for a SIM table input for consecutive input SIM centers and 0.10-m/z SIM windows

SIM Center	X						
	319	321	322	323	324	325	326
X.00	318.93–319.08	320.95–321.11	321.92–322.08	322.93–323.09	323.94–324.10	324.95–325.11	325.92–326.08
X.01	318.93–319.08	320.95–321.11	321.96–322.12	322.93–323.09	323.94–324.10	324.95–325.11	325.96–326.12
X.02	318.97–319.12	320.95–321.11	321.96–322.12	322.97–323.13	323.94–324.10	324.95–325.11	325.96–326.12
X.03	318.97–319.12	320.95–321.11	321.96–322.12	322.97–323.13	323.98–324.14	324.95–325.11	325.96–326.12
X.04	318.97–319.12	320.99–321.15	321.96–322.12	322.97–323.13	323.98–324.14	324.99–325.15	325.96–326.12

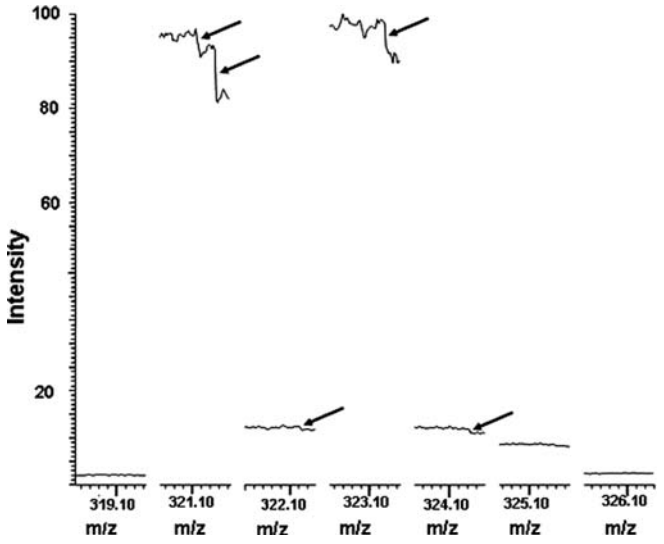

Fig. 3. SIM profile data collected from ^{18}O-enriched TMP samples. SIM acquisitions centered at 3XX.10 m/z and 0.16 m/z width acquired in the SIM-profile mode are shown. On the m/z axis each small division is 0.02. The SIM-profile mode varies the SIM center and records the average intensity of the data points within the SIM width. As the SIM center m/z increases, different digital settings are used in the average. Arrows indicate abrupt changes in signal intensity over narrow m/z ranges, which are attributed to a change in the identity of the digital m/z settings included in the recorded average.

Determination of isotope ratios by curve fitting data from scan acquisitions

Next we show that the potential for significant inaccuracies in the measurement of isotope ratios by SIM data acquisitions can be overcome by acquiring data in scan mode and integrating the area of the entire m/z peak. By acquiring data for the entire peak, as opposed to a small portion of the peak, the differential contributions of individual corresponding data points between the isotopic peaks become insignificant as shown in the simulation of Fig. 2. However, multiple possibilities for integrating the scan data exist with each possessing idiosyncratic strengths and weaknesses.

One common integration strategy is to sum each individual point comprising the peak over a range of 1.00/z, where z is the charge of the analyzed ion. This strategy includes the greatest number of data points for the analysis of the peak intensity. The major analytical difficulty with this approach is accounting for peak overlap, i.e., when adjacent peaks are not baseline separated. Signal overlap can contribute to both inaccuracies and imprecision in measured isotope ratios. With QMS, signal overlap occurs even below 500 m/z as shown in Fig. 1. Modern MALDI-TOF and quadrupole-TOF instruments have much higher mass resolutions, but even with these instruments peak

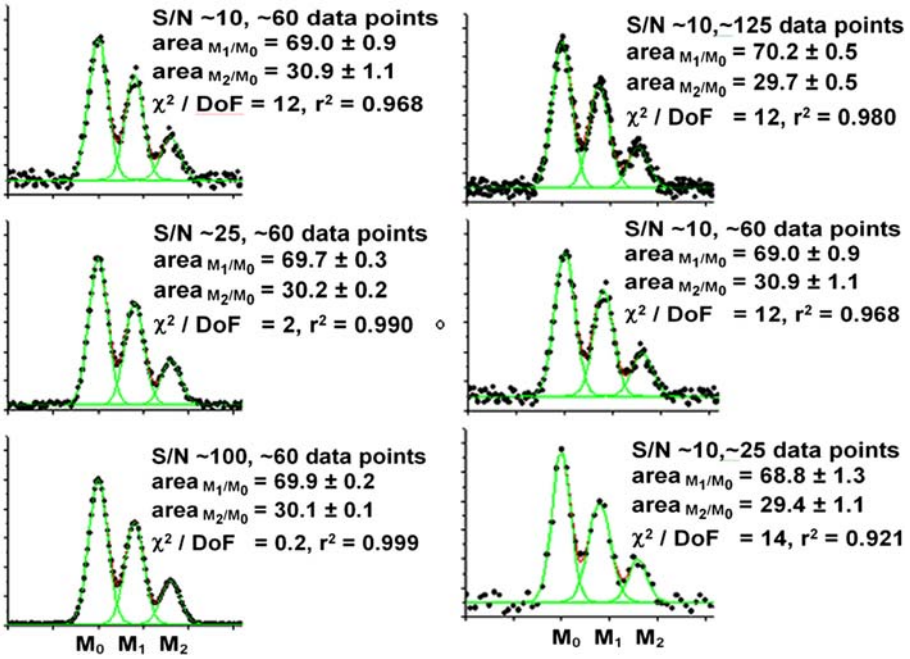

Fig. 4. Fits of sequential Gaussians can account for spillover with non-baseline-resolved peaks. The ability of the proposed protocol of fitting time-of-flight mass spectra to a series of Gaussian peaks to reproduce accurate isotope ratios as a function of signal/noise and data density is shown. In all cases the anticipated M_1/M_0 and M_2/M_0 ratios are 70 and 30, respectively. Typical simulations for six cases are shown along with the fits of the individual Gaussians. Simulations were repeated five times to generate the standard errors. As expected increasing S/N and numbers of data points increase the precision of the measurement. The simulation demonstrates that the method does not introduce a systematic inaccuracy. Other methods of analysis (e.g., using maximum peak intensity or summation of data points) introduce inaccuracies and decrease precision when there is substantial peak overlap.

overlap can become a problem at higher m/z or with multiply charged ions.

A second strategy which reduces the potential for significant signal overlap is to sum the data points corresponding to only the upper half of each individual peak [26]. This strategy is a compromise that increases the number of data points contributing to the measured peak intensity relative to SIM measurements which reduces the potential of inaccuracy introduced from mass granularity but limits the peak width analyzed to minimize signal overlaps. This protocol has inherent technical difficulties, however, in determining what constitutes the "upper half" which may lead to inaccuracies also.

We advocate fitting the scan data to an equation that describes a series of peaks separated by 1.000 m/z with identical peak shapes utilizing all of the scan data points acquired across the IIC, an approach adapted from NMR peak integration [27]. This method minimizes the contributions to uncertainty in the measured isotope ratio by mass granularity and peak overlap. An example is shown in Fig. 4 where simulated IDs with overlapping Gaussian peaks and added random errors are analyzed. The simulations show that with 60 data points/m/z and a signal/noise ratio of 25 that random noise will introduce an error of <0.5%. Analysis of these IDs also demonstrates that inaccuracies are introduced due to peak overlap by determining the area of the peaks by simple summation or by utilizing only the upper half of the peaks (data not shown).

The functional form used to define the peak shape is both instrument and tuning dependent, while the parameters of the functional form will be depend on both the tuning and the mass range of the ID to be analyzed. For QMS, Fig. 1 depicts the data and curve fit for the mass spectrum of [^{18}O]TMP to an equation describing the sum of five peaks. The functional form of the peak shape given in Eq. (1) was determined from the analysis of unlabeled TMP. Various functional forms were tried and the final form chosen provided both best fit of the profile scan mass spectrum and accurate natural-abundance values for M_1/M_0 and M_2/M_0. The fit to the equation yielded an R^2 of 0.9990. The fits for three analyses for each of three different TMP samples ranged from 0.9987 to 0.9991.

Comparison of the precision and accuracy of the SIM and Scan methods

To address the relative accuracy and precision of the isotope ratios determined by SIM and Scan analyses, several methods utilizing both SIM and Scan acquisition modes were used to calculate the isotope ratios for two separate ^{18}O-enriched TMP samples. Three separate SIM methods were utilized. The standard "SIM" method included data from the entire SIM m/z range. The "Common" method included only the data from the m/z ranges common to both peaks. The "SIM Max" method included only data that corresponded to the maximal ion intensity for each peak. These methods were applied to data acquired from SIM tables centered at both 32X.04 and 32X.08, where X can be either 1 or 3.

Four methods for determining peak intensity were applied to data acquired in the profile mode. The "Equation Fit" method fits the scan data to an equation describing a sum of five peaks as described above. The "Peak" method includes only the data point corresponding to the maximal intensity of each peak. The "$\frac{1}{2}$Sum" method sums

Table 3
Comparison of M_2/M_0 determined with different SIM and profile methods

SIM Center	32X.04	32X.04	32X.04	32X.08	32X.08	32X.08				
Method	SIM	SIM Overlap	SIM Peak Overlap	SIM	SIM Overlap	SIM Peak Overlap	Scan Eq. Fit	Scan Peak	Scan $\frac{1}{2}$Sum	Scan FSum
Sample 1										
Trial #1	N/D	N/D	N/D	1.045	1.031	1.028	1.053	1.044	1.051	1.057
Trial #2	N/D	N/D	N/D	1.048	1.033	1.027	1.042	1.017	1.041	1.049
Trial #3	N/D	N/D	N/D	1.051	1.038	1.035	1.048	1.030	1.047	1.054
Avg	N/D	N/D	N/D	1.048	1.034	1.030	1.048	1.030	1.046	1.053
Std. Dev.	N/D	N/D	N/D	0.003	0.003	0.004	0.006	0.013	0.005	0.004
Sample 2										
Trial #1	1.022	1.019	1.019	1.047	1.035	1.033	1.047	1.035	1.046	1.052
Trial #2	1.015	1.015	1.015	1.043	1.028	1.026	1.041	1.018	1.041	1.048
Trial #3	1.032	1.029	1.029	N/D	N/D	N/D	1.067	1.040	1.066	1.071
Avg	1.023	1.021	1.021	1.045	1.032	1.030	1.052	1.031	1.051	1.057
Std. Dev.	0.009	0.007	0.007	0.002	0.005	0.005	0.014	0.012	0.013	0.013
SIM Center	32X.04	32X.04	32X.04	32X.08	32X.08	32X.08				
Method	SIM	SIM Common	SIM Max	SIM	SIM Overlap	SIM Peak Overlap	Scan Eq. Fit	Scan Peak	Scan $\frac{1}{2}$Sum	Scan FSum
Sample 3										
Trial #1	1.023	1.020	1.020	1.048	1.033	1.031	1.040	1.017	1.039	1.046
Trial #2	1.029	1.028	1.028	1.043	1.027	1.026	1.044	1.041	1.043	1.048
Trial #3	1.017	1.017	1.017	N/D	N/D	N/D	1.038	1.019	1.037	1.046
Avg	1.023	1.022	1.022	1.045	1.030	1.029	1.041	1.026	1.040	1.046
Std. Dev.	0.006	0.006	0.006	0.004	0.004	0.004	0.003	0.013	0.003	0.001

all data points corresponding to the upper half of each peak. The "FSum" method sums all the data points for each peak within 0.5 m/z from the peak center. The results of calculating the ratio of peak intensities at $m/z = 321$ and 323 for each of the three [^{18}O]TMP samples are summarized in Table 3.

Precision is often more critical than accuracy for isotope ratio measurements. For example, in studies examining isotope ratios in several samples of the same molecule, identical m/z channels will be used for the analysis of all samples. Thus, errors in accuracy will remain constant throughout the study and cancel out in the final analysis. In such cases, precision and not accuracy will limit the utility of the instrument. SIM analysis, because it maximizes analysis time on the m/z values of maximal signal, is generally considered to provide the best precision. However, recognizing that temperature and other factors can result in drift of the mass calibration, these measurements should not be determined on separate days, when the mass axis calibration could vary by 0.02 m/z.

The precision achieved using the Equation Fit method of analyzing data acquired in profile mode compares favorably with the precision of the SIM methods. The standard deviation of the SIM methods for ratios near 1 ranged from 0.002 to 0.009 with a median value of 0.005 and a mode of 0.004. The standard deviations for the Equation Fit analysis of samples 1 and 3 are 0.003 and 0.006, respectively. This level of precision is comparable to that of the SIM analyses. The standard deviation for sample 2 (0.014) is substantially larger. However, this large value appears to result from an outlier point in the third trial, as evidenced by its abnormally large ratio for all three scan methods. Overall, precision comparable to that of SIM analysis appears readily attainable using the Equation Fit method. The worst precision was observed for ratios calculated using the Peak method. This observation is not surprising considering that the peak intensities come from a single data point acquired in profile mode. Precisions for the two sum methods were slightly better than that of the Equation Fit method, demonstrating that the data acquired in profile mode by the TSQ display had outstanding reproducibility overall. However, these sum methods would require a correction for peak overlap to maximize accuracy.

Unfortunately, no absolute standard of comparison exists to assess the accuracy of the various methods for isotope ratios near 1. The M_2/M_0 ratio calculated from the Equation Fit analysis was used as the standard for comparison for the other methods for two reasons. First, it minimizes two known sources of inaccuracy, mass granularity and peak overlap. Second, the method produces ratios for the intensity of $m/z = 322$ and 321 (M_1/M_0) in excellent agreement with the values expected due to the natural abundance of ^{2}H, ^{13}C, ^{15}N, and ^{17}O (Table 4). Thus, the method does not appear to introduce a new source of inaccuracy. The SIM methods using the 32X.08 SIM table and the $\frac{1}{2}$Sum profile method most closely approximated the Equation Fit values. The potential inaccuracy of the SIM methods is demonstrated again by noting the difference in the results using 32X.04 and 32X.08 SIM tables. The close correspondence of the $\frac{1}{2}$Sum method is not surprising as it holds the same advantages as the Equation Fit method but to a somewhat lesser extent. Although the $\frac{1}{2}$Sum method does not utilize all of the data points from profile acquisitions, it does utilize at least six data points for each peak. This number of data points appears to be sufficient to minimize sources of error from mass granularity. Additionally, because it excludes points at the peak edges, the $\frac{1}{2}$Sum method also minimizes error introduced from signal overlap which is detectable in the FSum analysis. The errors introduced by peak overlap will increase with both higher molecular masses and lower resolution.

Isotope ratio measurements by quadrupole instruments are usually most accurate when they are near unity [17]. This generalization results from the equal contribution of errors in background corrections to the intensity of each peak. For ratios far from unity, such contributions affect the less intense peak to a greater extent than the more intense peak, introducing artifacts into the measured ratios. However, measurement of such nonunity ratios is very useful for several applications such as nutritional trace labeling studies [28–30]. Additionally, measuring the predicted M_1/M_0 value represents an important internal control for judging the accuracy of an ESI–QMS quantitation method.

Samples of ^{18}O-enriched pGp allow these analyses to be made on a second molecule to test the general applicability of this technique. For pGp, M_1/M_0 is measured from the peaks at $m/z = 443$ and 442. The results are presented in Table 4. In all cases, the average measured values are in very close agreement with the predicted values, coming within 0.001 for a relative standard deviation of 0.021. Additionally, the precision of the measurements is satisfactory, with the standard deviation ranging from 0.001 to 0.004. Interestingly, the measured values for the M_2/M_0 relative intensity displayed the same absolute accuracy and precision as the M_1/M_0 ratios despite being only one-fourth the magnitude. This result suggests that the method can detect small levels of enrichment, even for very low natural abundance levels. The ability to detect such low enrichment may be extremely valuable for measuring the incorporation of isotopically enriched amino acids into proteins [31–33].

Overall, the results presented in Table 4 compare favorably with similar work for derivatized amino acids [34–36].

Table 4
Natural-abundance measurements for TMP and pGp using the Equation Fit profile method

	Predicted	n	Average	Standard deviation (SD)	Relative SD
TMP					
M_1/M_0	0.120	18	0.119	0.001	0.009
pGp					
M_1/M_0	0.133	40	0.133	0.004	0.034
M_2/M_0	0.030	20	0.029	0.001	0.021

These studies used ESI with either ion trap or QMS and fast atom bombardment ionization-QMS. The best results reported from these studies utilized ESI–QMS with separation of derivatized forms of the amino acids arginine and citrulline by HPLC occurring separately from the mass spectrometric analysis [34]. The results presented here indicate that a similar method involving offline HPLC purification combined with ESI–QMS analysis also yields extremely accurate and precise natural abundance for nucleotides.

Application to time-of-flight mass analyzers and tandem mass spectrometry

Acquiring QMS data in scan mode obviates the inaccuracies potentially introduced by SIM data acquisition. Time-of-flight mass analyzers inherently acquire data in scan mode where Gaussian peaks shapes are routinely obtained [37]. Time-of-flight mass analyzers have been adopted to ICP isotope ratio measurements [38,39] where the performance of quadrupole SIM and time-of-flight data acquisition have been compared [40]. Mass bias attributable to mass-dependent detection efficiencies can affect the accuracy of the measurements in time-of- flight instruments; however, these effects can be minimized [41,42].

Tandem mass spectrometry has been applied previously to the analysis of IDs [43,44]; however, these efforts were directed to characterizing positional isotopomers by fragmenting a single peak from the ID of the parent ion. There are three significant advantages to employing tandem mass spectrometry to the determination of isotope ratios from IDs. First, the potential for contamination is dramatically decreased; second, the background noise is reduced to near zero, enhancing the signal/noise and reducing the errors contributed by background subtraction; and third, the reduction in mass both reduces the contribution of natural-abundance isotopes and enhances the resolution of the peaks in the ID as shown in Fig. 5.

The determination of isotope ratios by tandem mass spectrometry faces four prominent objections. First, the fragmentation procedure should not induce a scrambling of the isotopic label. For the ^{18}O nucleotides this is not anticipated to be a problem, although it is a major consideration for identifying ^{2}H present in solvent-exchangeable positions [45]. Second, isotope effects on fragmentation can alter the measured isotopic composition in the product ion from that present in the precursor ion [46]. This will be a more significant problem with ^{2}H and when the isotopically labeled site results in a primary isotope effect on the major fragmentation pathway. In the nucleotide studies described, the remote ^{18}O kinetic isotope effects on fragmentation are anticipated to be significantly smaller than the experimental accuracy of the measurements. Third, isotopic fractionation can occur if the entire IIC of precursor ions is not passed through the first mass analyzer and collision chamber. This can be checked by obtaining the time-of-flight mass spectrum of the precursor cluster as a function of isolation width while using a minimal fragmentation energy. When increasing the isolation width results in no further change in the relative intensities of the peaks in the IIC, the accuracy of the isotope ratios can be tested by comparison to the predicted natural-abundance spectrum. In the accompanying paper the accuracy for peptide fragmentation is documented. Fourth, instrumental mass bias resulting from mass-dependent detection efficiencies can affect the accuracy of the measurements.

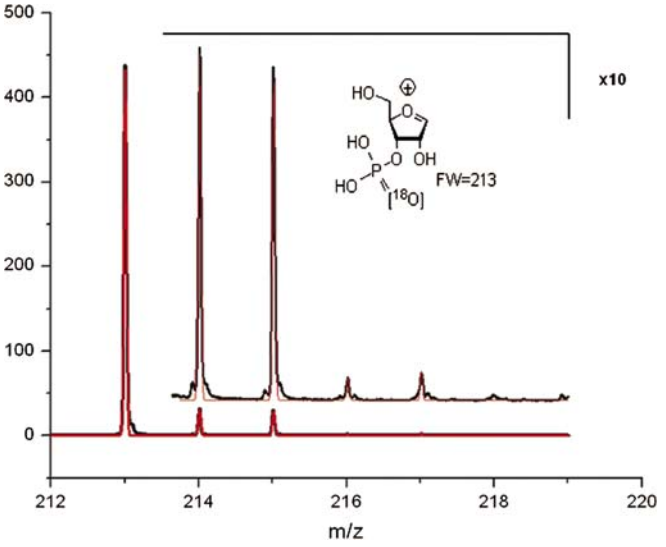

Fig. 5. Tandem mass spectrum of the protonated uracil product ion derived from 3′-UM[$^{18}O_1$]Puridine with the experimental isotopologue ion cluster fit to a series of five Gaussian peaks.

The ID obtained for the ribosyl-3-phosphate[+1] ion by fragmentation of the protonated IIC of 3′-UM[$^{18}O_1$]P is shown in Fig. 5. The nonlinear least squares fit of the ID to five sequential Gaussians separated by 1.00 m/z with identical peak widths is shown. No attempts were made to use only the top half as Gaussian peaks can be

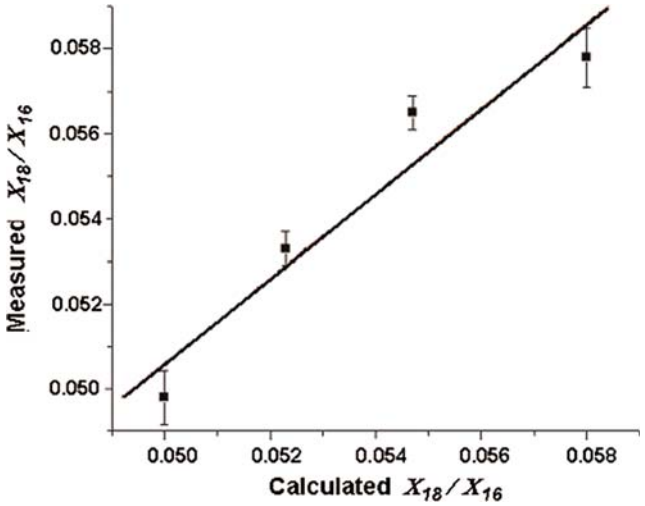

Fig. 6. Graph of X_{18}/X_{16} observed as calculated by a nonlinear least squares fit to Eq. (6) (solid squares) versus the value calculated based on mass balance.

integrated across the entire peak with minimal loss of precision [47]. The peak areas obtained for each Gaussian were fit to Eq. (5) with the mol fraction ratio (X_{18}/X_{16}), the only adjustable parameter in Excel using ''18O KIE calc from ID.xls'' included as Supplementary Material. The mol fraction ratio was varied systematically by sequential additions of 3′-UM[$^{18}O_1$]P which increases X_{18}/X_{16} of the analyzed solution. The result of these analyses is shown in Fig. 6. The linearity of the data and the standard deviations of the replicates indicate that the precision of the isotope ratios obtained from the product ion should be sufficient to permit heavy atom isotope effects to be determined on nucleotides. Similar results were obtained for the protonated base product ion when [1-^{18}O]uridine was analyzed (data not shown). The procedures described to obtain and analyze IDs by tandem MS for nucleotides (and peptides [22]) will permit heavy atom isotope effect studies to be conducted on these biomacromolecular substrates.

Acknowledgment

We appreciate the assistance of Steven Ingalls for assistance with data acquisition on the Finnigan TSQ 7000.

Appendix A. Supplementary data

Supplementary data associated with this article can be found, in the online version, at doi:10.1016/j.ab.2007.03.037.

References

[1] A. Fry, Heavy atom isotope effects in organic reaction mechanism studies, in: C.J. Collins, N.S. Bowman (Eds.), Isotope effects in chemical reactions, Van Nostrand-Reinhold, Princeton, N.J., 1970, pp. 364–414.
[2] W.W. Cleland, Determining the chemical mechanisms of enzyme-catalyzed reactions by kinetic studies, Adv. Enzymol. Relat. Areas Mol. Biol. 45 (1977) 273–387.
[3] M.H. O'Leary, Determination of heavy-atom isotope effects on enzyme-catalyzed reactions, Methods Enzymol. 64 (1980) 83–104.
[4] P.F. Cook (Ed.), Enzyme mechanism from isotope effects, CRC Press, Boca Raton, FL, 1991.
[5] V.L. Schramm, Enzymatic transition states and transition state analog design, Annu. Rev. Biochem. 67 (1998) 693–720.
[6] W.W. Cleland, The use of isotope effects to determine enzyme mechanisms, Arch. Biochem. Biophys. 433 (2005) 2–12.
[7] A. Kohen, H.H. Limbach (Eds.), Isotope effects in chemistry and biology, CRC, Boca Raton, FL, 2006.
[8] J. Bigeleisen, M. Wolfsberg, Theoretical and experimental aspects of isotope effects in chemical kinetics, Adv. Chem. Phys. 1 (1958) 15–76.
[9] V.L. Schramm, Enzymatic transition-state analysis and transition-state analogs, Methods Enzymol. 308 (1999) 301–355.
[10] O. Matsson, Isotope effects for exotic nuclei, in: A. Kohen, H.H. Limbach (Eds.), Isotope effects in chemistry and biology, CRC Press, Boca Raton, 2006, pp. 417–431.
[11] C.B. Sawyer, J.F. Kirsch, Kinetic isotope effects for reactions of methyl formate-methoxyl-^{18}O, J. Am. Chem. Soc. 95 (1973) 7375–7381.
[12] C.B. Sawyer, J.F. Kirsch, Kinetic isotope effects for the chymotrypsin catalyzed hydrolysis of ethoxyl-^{18}O labeled specific ester substrates, J. Am. Chem. Soc. 97 (1975) 1963–1964.
[13] B.J. Bahnson, V.E. Anderson, Crotonase-catalyzed b-elimination is concerted: A double isotope effect study, Biochemistry 30 (1991) 5894–5906.
[14] P.J. Berti, S.R. Blanke, V.L. Schramm, Transition state structure for the hydrolysis of NAD+ catalyzed by diphtheria toxin, J. Am. Chem. Soc. 119 (1997) 12079–12088.
[15] M.B. Goshe, Y.H. Chen, V.E. Anderson, Identification of the sites of hydroxyl radical reaction with peptides by hydrogen/deuterium exchange: Prevalence of reactions with the side chains, Biochemistry 39 (2000) 1761–1770.
[16] A.C. Seila, K. Okuda, S. Nunez, A.F. Seila, S.A. Strobel, Kinetic isotope effect analysis of the ribosomal peptidyl transferase reaction, Biochemistry 44 (2005) 4018–4027.
[17] I.S. Begley, B.L. Sharp, Characterisation and correction of instrumental bias in inductively coupled plasma quadrupole mass spectrometry for accurate measurement of lead isotope ratios, J. Anal. At. Spectrom. 12 (1997) 395–402.
[18] A.G. Cassano, V.E. Anderson, M.E. Harris, Analysis of solvent nucleophile isotope effects: Evidence for concerted mechanisms and nucleophilic activation by metal coordination in non-enzymatic and ribozyme catalyzed phosphodiester hydrolysis, Biochemistry 43 (2004) 10547–10559.
[19] N.M. Kaye, N.H. Zahler, E.L. Christian, M.E. Harris, Conservation of helical structure contributes to functional metal ion interactions in the catalytic domain of ribonuclease P RNA, J. Mol. Biol. 324 (2002) 429–442.
[20] E.L. Christian, D.S. McPheeters, M.E. Harris, Identification of individual nucleotides in the bacterial ribonuclease P ribozyme adjacent to the pre-tRNA cleavage site by short-range photo-cross-linking, Biochemistry 37 (1998) 17618–17628.
[21] K. Blaum, C. Geppert, P. Muller, W. Nortershauser, K. Wendt, B.A. Bushaw, Peak shape for a quadrupole mass spectrometer: Comparison of computer simulation and experiment, Int. J. Mass Spectrom. 202 (2000) 81–89.
[22] B. Wang, G. Sun, D.R. Anderson, M. Jia, S. Previs, and V.E. Anderson, Mass isotopomer distributions of peptide fragment ions by tandem mass spectrometry: Quantitation of low levels of deuterium incorporation, Anal. Biochem. submitted (2007).
[23] S.P. Gygi, B. Rist, S.A. Gerber, F. Turecek, M.H. Gelb, R. Aebersold, Quantitative analysis of complex protein mixtures using isotope-coded affinity tags, Nat. Biotechnol. 17 (1999) 994–999.
[24] A.G. Cassano, V.E. Anderson, M.E. Harris, Evidence for direct attack by hydroxide in phosphodiester hydrolysis, J. Am. Chem. Soc. 124 (2002) 10964.
[25] H. Park, G.G. Girdaukas, D.B. Northrop, Effect of pressure on a heavy-atom isotope effect of yeast alcohol dehydrogenase, J. Am. Chem. Soc. 128 (2006) 1868–1872.
[26] I.S. Begley, C.M. Scrimgeour, High-precision d^{2}H and d^{18}O measurement for water and volatile organic compounds by continuous-flow pyrolysis isotope ratio mass spectrometry, Anal. Chem. 69 (1997) 1530–1535.
[27] A. Kumar, C.H. Sotak, C.L. Dumoulin, G.C. Levy, Software for deconvolution of overlapping spectral peaks and quantitative analysis by carbon-13 Fourier transform NMR spectroscopy, Computer-Enhanced Spectroscopy 1 (1983) 107–114.
[28] S. Reid, C. Shackleton, K. Wu, S. Kaempfer, M.K. Hellerstein, Liquid chromatography/mass spectrometry of plasma glucose and secreted glucuronate for metabolic studies in humans, Biomed. Environ. Mass Spectrom. 19 (1990) 535–540.
[29] B.W. Patterson, X.J. Zhang, Y. Chen, S. Klein, R.R. Wolfe, Measurement of very low stable isotope enrichments by gas chromatography/mass spectrometry: Application to measurement of muscle protein synthesis, Metabolism 46 (1997) 943–948.
[30] J. Katanik, B.J. McCabe, D.Z. Brunengraber, V. Chandramouli, F.J. Nishiyama, V.E. Anderson, S.F. Previs, Measuring gluconeogenesis using a low dose of ^2H_2O: Advantage of isotope fractionation during gas chromatography, Am. J. Physiol. Endocrinol. Metab. 284 (2003) E1043–E1048.

[31] C. Papageorgopoulos, K. Caldwell, C. Shackleton, H. Schweingrubber, M.K. Hellerstein, Measuring protein synthesis by mass isotopomer distribution analysis (MIDA), Anal. Biochem. 267 (1999) 1–16.
[32] C. Papageorgopoulos, K. Caldwell, H. Schweingrubber, R.A. Neese, C.H. Shackleton, M. Hellerstein, Measuring synthesis rates of muscle creatine kinase and myosin with stable isotopes and mass spectrometry, Anal. Biochem. 309 (2002) 1–10.
[33] R. Busch, Y.K. Kim, R.A. Neese, V. Schade-Serin, M. Collins, M. Awada, J.L. Gardner, C. Beysen, M.E. Marino, L.M. Misell, M.K. Hellerstein, Measurement of protein turnover rates by heavy water labeling of nonessential amino acids, Biochim. Biophys. Acta 1760 (2006) 730–744.
[34] F.M. Lagerwerf, R.M. Wever, H.J. van Rijn, C. Versluis, W. Heerma, J. Haverkamp, H.A. Koomans, T.J. Rabelink, P. Boer, Assessment of nitric oxide production by measurement of [^{15}N]citrulline enrichment in human plasma using high-performance liquid chromatography-mass spectrometry, Anal. Biochem. 257 (1998) 45–52.
[35] H.M. van Eijk, D.R. Rooyakkers, P.B. Soeters, N.E. Deutz, Determination of amino acid isotope enrichment using liquid chromatography-mass spectrometry, Anal. Biochem. 271 (1999) 8–17.
[36] S. Hess, J. van Beek, L.K. Pannell, Acid hydrolysis of silk fibroins and determination of the enrichment of isotopically labeled amino acids using precolumn derivatization and high-performance liquid chromatography-electrospray ionization-mass spectrometry, Anal. Biochem. 311 (2002) 19–26.
[37] M. Guilhaus, Principles and instrumentation in time-of-flight mass spectrometry. Physical and instrumental concepts, J. Mass Spectrom. 30 (1995) 1519–1532.
[38] X. Tian, H. Emteborg, F.C. Adams, Analytical performance of axial inductively coupled plasma time of flight mass spectrometry (ICP-TOFMS), J. Anal. At. Spectrom. 14 (1999) 1807–1814.
[39] I.L. Koumenis, M.L. Vestal, A.L. Yergey, S. Abrams, S.N. Deming, T.W. Hutchens, Quantitation of metal isotope ratios by laser desorption time-of-flight mass spectrometry, Anal. Chem. 67 (1995) 4557–4564.
[40] M. Vazquez Pelaez, J.M. Costa-Fernandez, A. Sanz-Medel, Critical comparison between quadrupole and time-of-flight inductively coupled plasma mass spectrometers for isotope ratio measurements in elemental speciation, J. Anal. At. Spectrom. 17 (2002) 950–957.
[41] J. Axelsson, E. Scrivener, D.M. Haddleton, P.J. Derrick, Mass discrimination effects in an ion detector and other causes for shifts in polymer mass distributions measured by matrix-assisted laser desorption/ionization time-of-flight mass spectrometry, Macromolecules 29 (1996) 8875–8882.
[42] K. Benkhedda, H. Goenaga Infante, F.C. Adams, Determination of total lead and lead isotope ratios in natural waters by inductively coupled plasma time-of-flight mass spectrometry after flow injection on-line preconcentration, Anal. Chim. Acta 506 (2004) 137–144.
[43] F.M. Jeffrey, J.S. Roach, C.J. Storey, A.D. Sherry, C.R. Malloy, ^{13}C isotopomer analysis of glutamate by tandem mass spectrometry, Anal. Biochem. 300 (2002) 192–205.
[44] A. Rantanen, J. Rousu, J.T. Kokkonen, V. Tarkiainen, R.A. Ketola, Computing positional isotopomer distributions from tandem mass spectrometric data, Metab. Eng. 4 (2002) 285–294.
[45] J.K. Hoerner, H. Xiao, A. Dobo, I.A. Kaltashov, Is there hydrogen scrambling in the gas phase? Energetic and structural determinants of proton mobility within protein ions, J. Am. Chem. Soc. 126 (2004) 7709–7717.
[46] J.R. Green, R.G. Cooks, Inverse heavy-atom kinetic isotope effects in chloroalkanes, J. Phys. Chem. A 108 (2004) 10039–10043.
[47] E.H. Piepmeier, Improving the precision of the integral of a transient absorbance peak, Anal. Chem. 48 (1976) 1296–1300.
[48] J. Yergey, A general approach to calculating isotopic distributions for mass spectrometry, Int. J. Mass Spectrom. Ion Phys. 52 (1983) 337–349.